Journal of ELECTRONIC MATERIALS, Vol. 42, No. 3, 2013
DOI: 10.1007/s11664-012-2370-5

Creation of Yb_2O_3 Nanoprecipitates Through an Oxidation Process in Bulk Yb-Filled Skutterudites

JUAN DING,[1,2] HUI GU,[1] PENGFEI QIU,[3] XIHONG CHEN,[3] ZHEN XIONG,[3] QIANG ZHENG,[1] XUN SHI,[3] and LIDONG CHEN[3,4]

1.—State Key Laboratory of High Performance Ceramics and Superfine Microstructure, Shanghai Institute of Ceramics, Chinese Academy of Sciences, Shanghai 200050, China. 2.—University of Chinese Academy of Sciences, Beijing 100049, China. 3.—CAS Key Laboratory of Materials for Energy Conversion, Shanghai Institute of Ceramics, Chinese Academy of Sciences, 1295 Dingxi Road, Shanghai 200050, China. 4.—e-mail: cld@mail.sic.ac.cn

An approach to introduce *in situ* nanoprecipitates into bulk filled skutterudites is developed through controlling the oxidation process of the fillers. $Yb_{0.3}Co_4Sb_{12}$ is selected as the base material, and prolonged oxidation at high temperatures in sealed quartz tubes under a low pressure of oxygen leads to the formation of Yb_2O_3 nanoinclusions. Transmission electron microscopy shows that the Yb_2O_3 nanoprecipitates are created within the skutterudite crystal grains through an internal oxidation mechanism. With increased time of oxidation, the amount of Yb_2O_3 nanoprecipitates is increased and the nanoprecipitates are more uniformly distributed in the matrix. For the samples oxidized for 10 days, the lattice thermal conductivity is reduced by about 19% at 850 K compared with the $Yb_{0.3}Co_4Sb_{12}$ matrix. The reduction in the lattice thermal conductivity originates from additional phonon scattering by the Yb_2O_3 nanoprecipitates, leading to a maximum ZT of 1.3.

Key words: Thermoelectric, filled skutterudite, nanocomposites

INTRODUCTION

Co_4Sb_{12}-based filled skutterudites have received great attention as promising thermoelectric materials due to their low lattice thermal conductivity (κ_L) and excellent electrical transport properties.[1–6] There are two large voids in the unit cell of skutterudites, and they can be filled by foreign species.[1,2] The filler atoms are loosely bonded with the neighboring Sb atoms, and their vibrations strongly scatter low-frequency thermal phonons and thereby greatly suppress κ_L, which, in turn, leads to an improvement in the dimensionless thermoelectric figure of merit (ZT).[1,2] Currently, rare-earth,[7–12] alkaline-earth,[13,14] and alkaline-metal[15] filled skutterudites have been systematically studied, and ZT values above unity have been reported, showing great potential in applications as mid- to high-temperature thermoelectric generators. Among these filled skutterudites, $Yb_xCo_4Sb_{12}$ is regarded as one of the best *n*-type single-filled skutterudites with excellent thermoelectric performance. In YbxCo$_4$Sb$_{12}$, the highest filling fraction x is estimated to be about 0.2,[7,16] within the range 0.15 to 0.35 of x values for fillers with charge state +2.[3–5] It is well known that nanoparticles or nanophases inside the crystal grains are believed to greatly reduce the lattice thermal conductivity and thereby further enhance the thermoelectric performance by introducing additional phonon defect scattering.[17–25] Zhao et al.[21] successfully introduced Yb_2O_3 nanoparticles into $Yb_xCo_4Sb_{12}$ using an *in situ* reaction method to show a significantly improved thermoelectric performance. This work suggests a new possibility of obtaining high ZT values in skutterudites by a cooperative effect of the fillers in the skutterudite voids and finely dispersed nanoinclusions in grains or at grain boundaries. In reality, most of the Yb oxide particles are aggregated at grain boundaries and only a very small amount of oxide particles are observed inside the grains of

(Received April 23, 2012; accepted November 19, 2012; published online January 4, 2013)

skutterudites.[21] This can adversely affect the electrical transport properties. Furthermore, detailed understanding concerning the distribution, evolution mechanism, and the effect of the *in situ* nanoparticles or nanoprecipitates on the thermoelectric properties is still uncertain and needs to be clarified in order to further optimize the thermoelectric performance of skutterudite nanocomposites. One of the greatest challenges for thermoelectric nanocomposites is to grow and fabricate bulk samples with nanoparticles uniformly distributed.

In this work, we attempted to introduce nano-Yb_2O_3 particles into $Yb_{0.3}Co_4Sb_{12}$ *in situ* through an oxidation process to achieve partial filler oxidization in an oxygen atmosphere. Samples were oxidized at high temperatures in sealed tubes with a very low amount of oxygen gas. Due to the very low formation energy, a fraction of the Yb fillers are oxidized to Yb_2O_3, which subsequently forms a finely dispersed nanophase throughout the skutterudite matrix. The subgrain microstructure of the resulting samples was examined by transmission electron microscopy (TEM), aiming to shed light on the mechanism of the microstructure evolution. Finally, the effect of the *in situ*-formed nanoinclusions on the thermoelectric properties was evaluated.

EXPERIMENTAL PROCEDURES

In this study, high-purity cobalt powders (99.99%), antimony shots (99.9999%), and ytterbium ingots (99.95%) were used as raw materials. A polycrystalline $Yb_{0.3}Co_4Sb_{12}$ (nominal composition) sample was prepared by the process of melting (1353 K) and annealing (1073 K, 7 days) followed by spark plasma

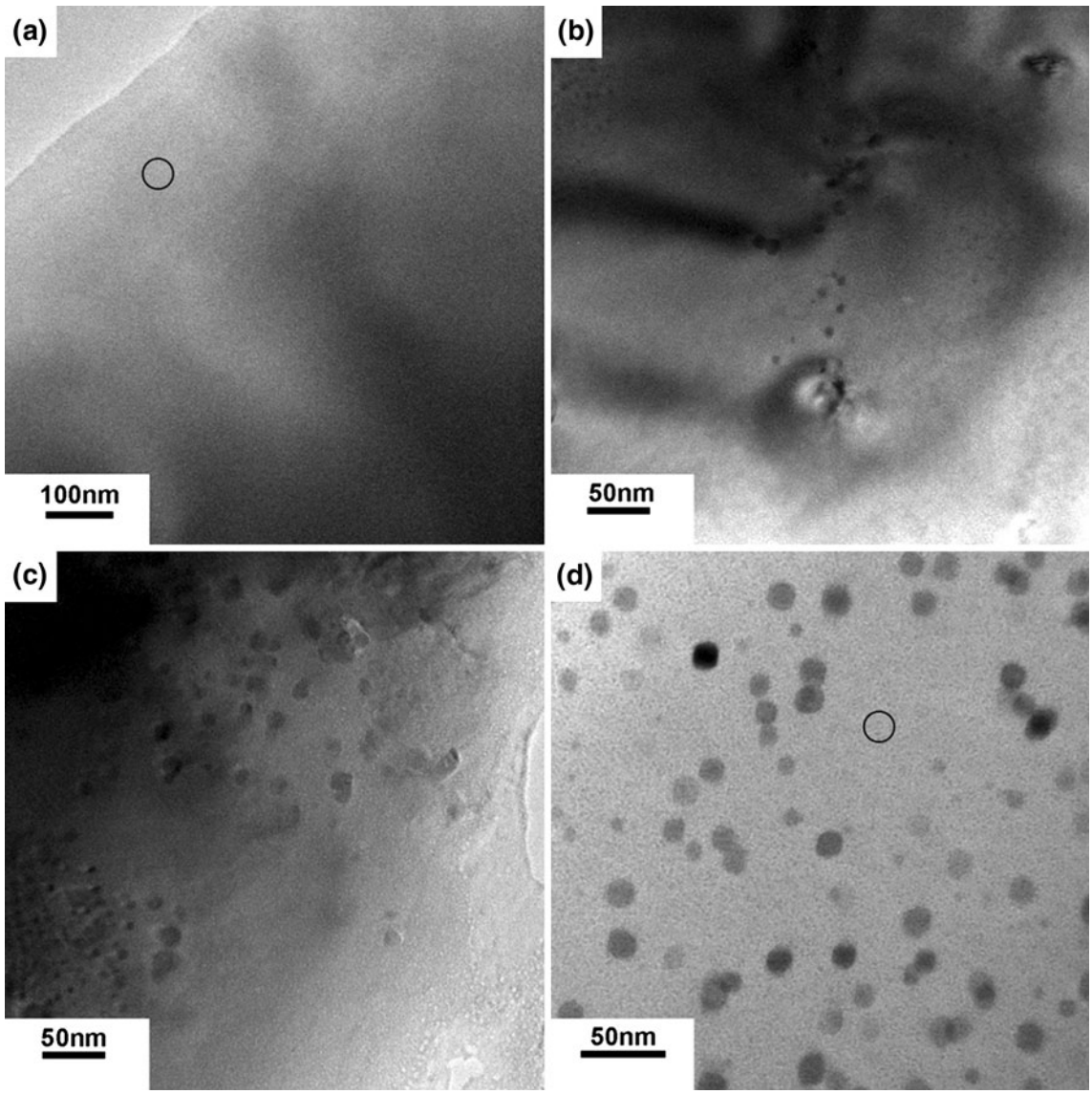

Fig. 1. Bright-field (BF) images for samples (a) 0.3-0, (b) 0.3-10, (c) 0.3-20, and (d) 0.3-30. The nano-Yb_2O_3 precipitates are clearly observed after the oxidation process. The marked circle areas were selected for EDXS analysis, shown in Fig. 4b.

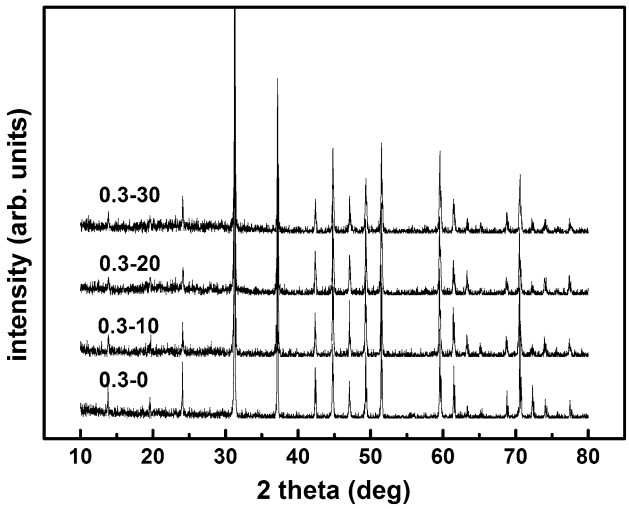

Fig. 2. XRD patterns for all samples.

sintering (SPS; 873 K, 5 min, 60 MPa). Pellet samples sintered by SPS were cut into four pieces. Three of them were sealed in quartz tubes under an oxygen pressure of about 2.5 kPa, and then annealed at 873 K for 10 days, 20 days, and 30 days. All the samples are labeled by their nominal Yb content and the oxidation time; For example, 0.3-30 stands for the $Yb_{0.3}Co_4Sb_{12}$ sample oxidized for 30 days.

A small part of each oxidized sample was ground to a fine powder for x-ray diffraction (XRD, Rint2000; Rigaku) analysis. The electrical conductivity (σ) was measured by a standard four-probe method, and the Seebeck coefficient (S) was measured under temperature differences between 1 K and 10 K using a ZEM-3 (ULVAC-RIKO) under protective He gas. Measurement of thermal diffusivity (λ) was carried out in flowing Ar atmosphere by the laser flash method (Netzsch LFA-427). The specific heat C_P was measured in an argon atmosphere using Shimadzu DSC-50. The measured heat capacity values increase almost linearly from 0.22 J/g K at room temperature to 0.235 J/g K at 850 K. Thermal conductivity (κ) was calculated using the relationship $\kappa = \rho\lambda C_P$, where ρ is the sample density. The estimated measurement accuracies of thermoelectric parameters are as follows: 5% for σ, 7% for S, and 10% for thermal conductivity. TEM specimens were prepared by argon ion milling after mechanical slicing, polishing, and dimpling. An electron microscope (JEM 2100F) operating at 200 keV was equipped with an energy-dispersive x-ray spectroscopy (EDXS) system (Link/ISIS; Oxford Instruments) for local chemical analysis. High-angle dark-field (HADF) imaging and elemental line profiling with EDXS were carried out in an electron microscope (FEI Tecnai-F30) operated at 300 keV.

RESULTS AND DISCUSSION

Figure 1 shows the evolution of the subgrain microstructure for all $Yb_{0.3}Co_4Sb_{12}$ samples. TEM results show no nanoprecipitates observed in the nonoxidized sample (marked as 0.3-0), while there are numerous nanoprecipitates in all oxidized $Yb_{0.3}Co_4Sb_{12}$ samples. As the oxidation time increases, the density of nanoprecipitates increases. In addition, while nanoprecipitates are nonuniformly distributed in samples 0.3-10 and 0.3-20, they are much more uniformly distributed in sample 3-30 (Fig. 1). Furthermore, as shown in Fig. 1b–d, the size of the nanoprecipitates exhibits a tendency to grow from about 5 nm to 15 nm as the oxidation time increases from 10 days to 30 days. Figure 2 shows the XRD data for all samples. Only the skutterudite phase is observed in our Yb-filled skutterudite, and no obvious impurity phases are found in the oxidized samples. This might be explained by the low percentage of nanoimpurity particles in the skutterudite composites, which is beyond the measurement accuracy of our XRD system.

To identify the chemical content of the nanoprecipitates, chemical component analysis was carried out. Apart from a large amount of nanoprecipitates with size around 10 nm to 20 nm, the SEM image shows also some large impurity particles with size around 100 nm to 200 nm (Fig. 3a), which could result from the segregation of impurities. As shown in Fig. 3b, two precipitates with size close to 10 nm are directly visualized by the HADF image, which is highlighted from the relatively low-Z background. Elemental profiles across one such nanoprecipitate measured by an EDXS line scan marked in the HADF image are plotted in Fig. 3c. They reveal that the nanoprecipitate is rich in Yb, while the content of elements Sb and Co is relatively low. The HAADF profile (Fig. 3d) gives a similar intensity variation for this nanoparticle. The increased intensity at positions 5 nm to 15 nm shown in Fig. 3b indicates the enhanced average atomic mass in this area. The amount of elemental oxygen in the nanoparticle could not be determined by EDXS, since it has low sensitivity for detection of light elements. Nevertheless, the HRTEM image in Fig. 3e shows the existence of nanoprecipitates with sizes around 10 nm. Figure 3f shows a diffractogram created by fast Fourier transformation (FFT) for this nanoprecipitate. It corresponds to the [011] zone-axis diffraction pattern of the body-centered cubic Yb_2O_3 phase. This nanoprecipitate is orientated relative to the matrix with the relation $(013)_{CoSb_3}//(22-2)_{Yb_2O_3}$.

The existence of Yb_2O_3 nanoprecipitates in the oxidized samples could be understood as a result of partial oxidization of Yb fillers in the skutterudite structure. In the as-prepared $Yb_{0.3}Co_4Sb_{12}$ filled skutterudite, almost all the Yb atoms fill cages of the structure. When the $Yb_{0.3}Co_4Sb_{12}$ sample is placed in a tube containing oxygen and heated to high temperatures, a fraction of the Yb fillers escape from the skutterudite cages and react with oxygen to form Yb_2O_3 oxide. This, of course, leads to a reduced filling fraction in the voids. This is confirmed by the variation of the lattice constant

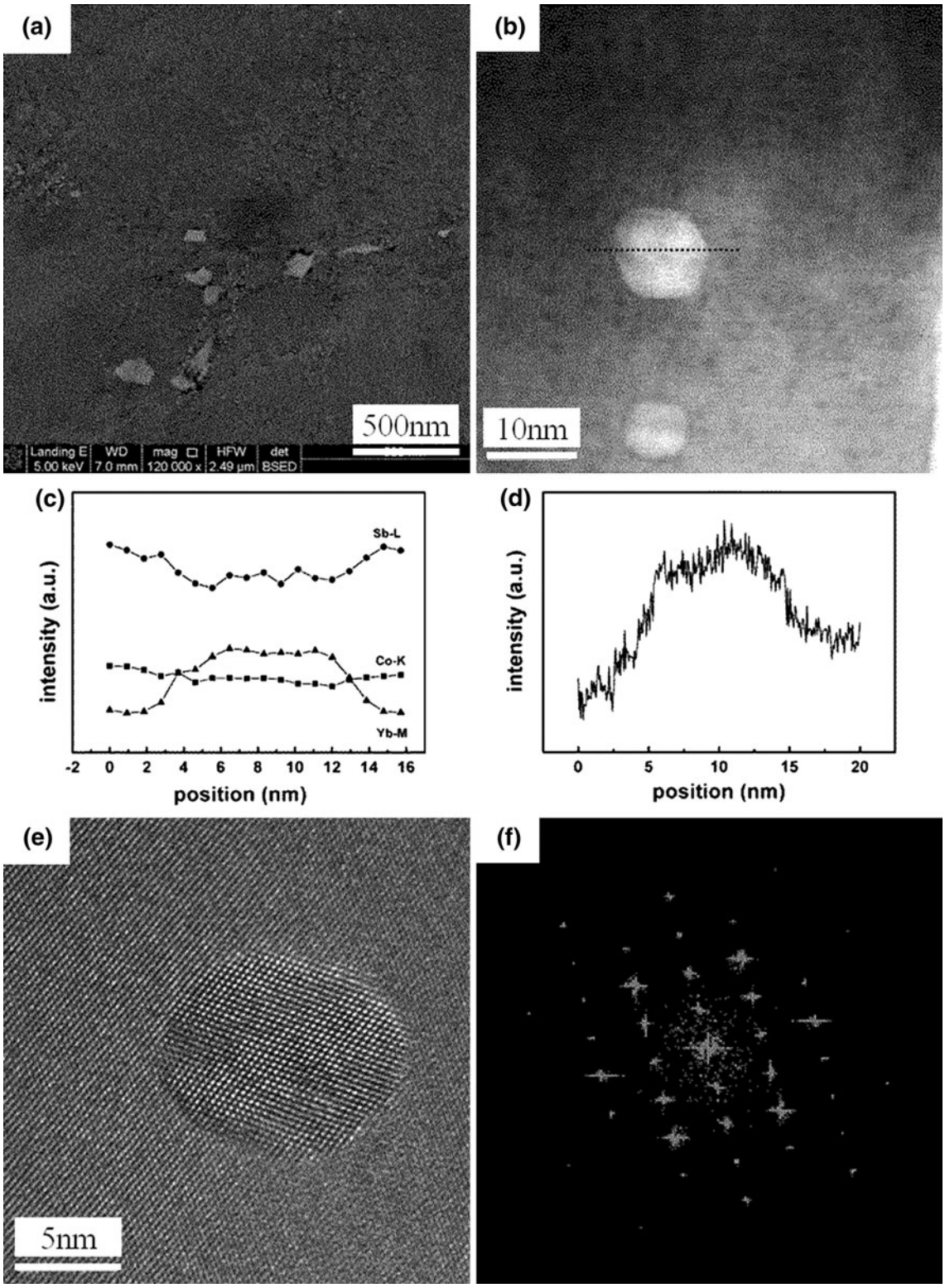

Fig. 3. The existence of nano-precipitates in the matrix of sample 0.3-30 visualized by (a) SEM image, (b) HADF image, (c) concentration profiles resulting from the EDXS line scan in Fig. 3b, (d) HAADF profile in Fig. 3b along the dotted line shown in Fig. 3b, and (e) in HRTEM image to show the nanoprecipitate with size around 10 nm with (f) FFT diagram showing its [011] zone-axis pattern of Yb_2O_3.

calculated from high-angle XRD data (Fig. 4a). The lattice constant initially slowly decreases with increasing oxidation time up to 20 days and then drops rapidly with further increase of oxidation time to 30 days. The increased density of Yb_2O_3 precipitates shown in Fig. 1 is consistent with this

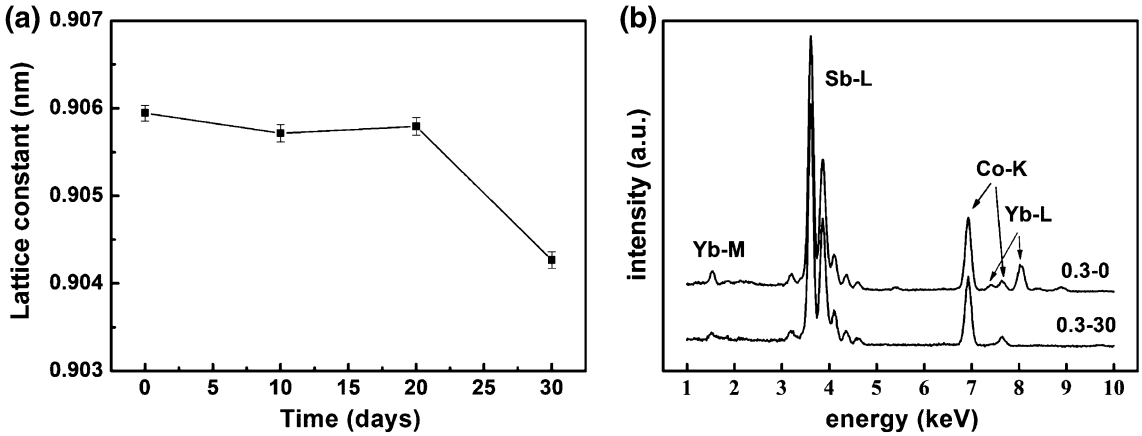

Fig. 4. (a) Lattice constant as a function of oxidation time for all samples. (b) EDXS spectra for the selected areas shown in Fig. 1a, d. The Yb EDXS spectral intensity is normalized by the intensities of Co K and Sb L peaks.

trend. Moreover, as shown in Fig. 4b, EDXS analysis detects a significantly decreased intensity of Yb L and Yb M peaks for the oxidized sample, while the intensity changes for Co K and Sb L peaks are very small.

The created Yb_2O_3 nanoprecipitates are expected to scatter lattice phonons and reduce the lattice and electronic thermal conductivities shown in Fig. 5a, b. Here, κ_L was estimated by subtracting the electronic contribution from the total thermal conductivity, according to the Wiedemann–Franz law, $\kappa_E = L\sigma T$. The Lorenz number (L) can be calculated by[25]

$$L = \left(\frac{k_B}{e}\right)^2 \left[\frac{3F_0(\eta)F_2(\eta) - 4F_1^2(\eta)}{F_0^2(\eta)}\right], \qquad (1)$$

where k_B is the Boltzmann constant, e is the elementary charge, η is the reduced Fermi energy, and the $F_n(\eta)$ are the Fermi–Dirac integrals. Since the Yb fillers that escaped from the voids of the skutterudite structure could change the electron concentration, we first calculate the Fermi energy and Fermi–Dirac integrals using the measured thermopower under the assumption of a single parabolic band and charge carriers at 300 K being dominantly scattered by acoustic phonons. Having the Fermi–Dirac integrals, we then calculate the Lorenz number using Eq. 1. The thus-obtained L values are $1.85 \times 10^{-8}\ V^2\ K^{-2}$ for sample 0.3-0, $1.86 \times 10^{-8}\ V^2\ K^{-2}$ for sample 0.3-10, $1.78 \times 10^{-8}\ V^2\ K^{-2}$ for sample 0.3-20, and $1.74 \times 10^{-8}\ V^2\ K^{-2}$ for sample 0.3-30. The total thermal conductivity is shown in Fig. 5b, and the lattice thermal conductivity is plotted in Fig. 5a. Except for sample 0.3-30, the calculated lattice thermal conductivities display a monotonically decreasing trend with increasing temperature. This indicates that the bipolar contribution is small in these samples. For sample 0.3-30, due to the large amount of Yb fillers lost from the voids, the bipolar effect seems much larger than in the other samples and the lattice thermal conductivity increases at temperatures above about 650 K. Based on Fig. 5a, the effect of oxygen annealing is as follows: the lattice thermal conductivity κ_L first decreases, reaches a minimum value after 10 days of oxidation, and finally increases with increasing oxidation time. As the exposure time to oxygen increases, the amount of Yb_2O_3 nanoprecipitates increases and the concentration of Yb fillers in the voids decrease. This is also partly confirmed by the decreased electrical conductivity and the enhanced absolute Seebeck coefficient shown in Fig. 5c, d. While the Yb_2O_3 nanoprecipitates scatter lattice phonons and reduce κ_L, the loss of Yb fillers from the skutterudite cages reduces the phonon resonant scattering and thus enhances the lattice thermal conductivity. These two competing effects are revealed in the observed trend of κ_L shown in Fig. 5a. Based on our results, the optimal oxidization time is estimated as around 10 days. For sample 0.3-10, the κ_L at 850 K is about 19% lower than that of sample 0.3-0, leading to a maximum ZT value of 1.3 at 850 K. This value is 10% higher than that of sample 0.3-0. Furthermore, the oxidized sample 0.3-10 shows a ZT improvement in the whole temperature range (Fig. 5e), indicating the possibility of large energy conversion efficiency for our nanocomposite samples when used in real thermoelectric (TE) applications.

CONCLUSIONS

We report on the effect of *in situ* nanoscale secondary phases in crystal grains of skutterudites. Through control of the oxidation process, the amount, size, and distribution of Yb_2O_3 nanoprecipitates can be well tuned. With increasing oxidization time, the amount of Yb_2O_3 nanoprecipitates is increased and they show a uniform distribution in the skutterudite matrix. For sample 0.3-10, significant suppression of κ_L is observed due to additional phonon scattering by the Yb_2O_3 nanoprecipitates, leading to enhanced ZT values over the entire investigated tempera-

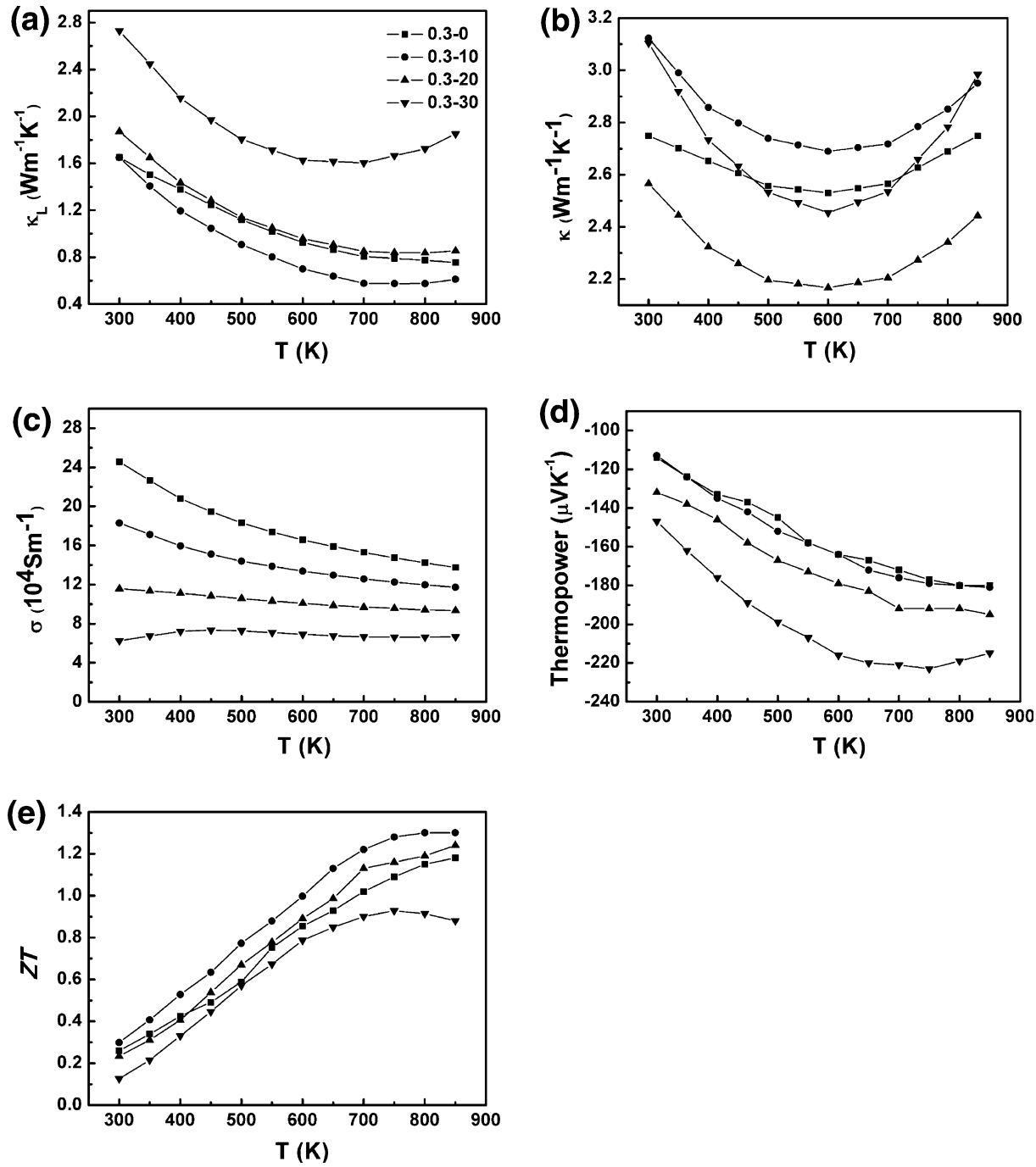

Fig. 5. Temperature dependence of (a) lattice thermal conductivity, (b) total thermal conductivity, (c) electrical conductivity, (d) Seebeck coefficient, and (e) the dimensionless thermoelectric *ZT* values for all the samples.

ture range. The thermoelectric properties could be further improved by adjusting the oxidation process (e.g., temperature, oxidation time, or oxygen pressure).

ACKNOWLEDGEMENTS

J.D. and H.G. would like to thank the Center for Nano-science and Technology, Xiamen University for equipment support. X.S. and L.C. would like to thank Prof. Ctirad Uher, University of Michigan for continuous encouragement and help. The authors acknowledge financial support from the NSFC (Project Nos. 11179013 and 51102260) and Shanghai Science and Technology Commission (Pujiang Program with No. 11PJ1410200 and the Nanotechnology Project with No. 11nm 0502800).

REFERENCES

1. C. Uher, *Semiconductors and Semimetals*, vol. 69, ed. T.M. Trit (New York: Academic), pp. 139–253.
2. B.C. Sales, D. Mandrus, and R.K. Williams, *Science* 272, 1325 (1996).
3. X. Shi, S.Q. Bai, L. Xi, J. Yang, W. Zhang, and L. Chen, *J. Mater. Res.* 26, 1745 (2011).
4. X. Shi, J. Yang, J.R. Salvador, M.F. Chi, J.Y. Cho, H. Wang, S.Q. Bai, J.H. Yang, W.Q. Zhang, and L.D. Chen, *J. Am. Chem. Soc.* 133, 7837 (2011).
5. X. Shi, H. Kong, C.P. Li, C. Uher, J. Yang, J.R. Salvador, H. Wang, L. Chen, and W. Zhang, *Appl. Phys. Lett.* 92, 182101 (2008).
6. G. Rogl, A. Grytsiv, E. Bauer, P. Rogl, and M. Zehetbauer, *Intermetallics* 18, 394 (2010).
7. G.S. Nolas, M. Kaeser, R.T. Littleton, and T.M. Tritt, *Appl. Phys. Lett.* 77, 1855 (2000).
8. D.T. Morelli, G.P. Meisner, B.X. Chen, S.Q. Hu, and C. Uher, *Phys. Rev. B* 56, 7376 (1997).
9. G.S. Nolas, J.L. Cohn, and G.A. Slack, *Phys. Rev. B* 58, 164 (1998).
10. A. Grytsiv, P. Rogl, S. Berger, C. Paul, E. Bauer, C. Godart, B. Ni, M.M. Abd-Elmeguid, A. Saccone, R. Ferro, and D. Kaczorowski, *Phys. Rev. B* 66, 0944411 (2002).
11. Y.Z. Pei, S.Q. Bai, X.Y. Zhao, W. Zhang, and L.D. Chen, *Solid State Sci.* 10, 1422 (2008).
12. V.L. Kuznetsov, L.A. Kuznetsova, and D.M. Rowe, *J. Phys. Condens. Matter* 29, 5035 (2003).
13. L.D. Chen, T. Kawahara, X.F. Tang, T. Goto, T. Hirai, J.S. Dyck, W. Chen, and C. Uher, *J. Appl. Phys.* 90, 1864 (2001).
14. M. Puyet, B. Lenoir, A. Dauscher, M. Dehmas, C. Stiewe, and E. Muller, *J. Appl. Phys.* 95, 4852 (2004).
15. Y.Z. Pei, L.D. Chen, W. Zhang, X. Shi, S.Q. Bai, X.Y. Zhao, Z.G. Mei, and X.Y. Li, *Appl. Phys. Lett.* 89, 221107 (2006).
16. J. Yang, Q. Hao, H. Wang, Y.C. Lan, Q.Y. He, A. Minnich, D.Z. Wang, J.A. Harriman, V.M. Varki, M.S. Dresselhaus, G. Chen, and Z.F. Ren, *Phys. Rev. B* 80, 115329 (2009).
17. L.D. Chen, X. Chen, and S.Q. Bai, *J. Inorg. Mater.* 25, 561 (2010).
18. B. Poudel, Q. Hao, Y. Ma, Y. Lan, A. Minnich, B. Yu, X. Yan, D. Wang, A. Muto, D. Vashaee, X. Chen, J. Liu, M.S. Dresselhaus, G. Chen, and Z.F. Ren, *Science* 320, 634 (2008).
19. X.W. Wang, H. Lee, Y.C. Lan, G.H. Zhu, G. Joshi, D.Z. Wang, J. Yang, A.J. Muto, M.Y. Tang, J. Klatsky, S. Song, M.S. Dresselhaus, G. Chen, and Z.F. Ren, *Appl. Phys. Lett.* 93, 193121 (2008).
20. Z. Xiong, X.Y. Huang, X.H. Chen, J. Ding, and L.D. Chen, *Scr. Mater.* 62, 93 (2010).
21. X.Y. Zhao, X. Shi, L.D. Chen, W. Zhang, S.Q. Bai, Y.Z. Pei, X.Y. Li, and T. Goto, *Appl. Phys. Lett.* 89, 092121 (2006).
22. H. Li, X.F. Tang, Q.J. Zhang, and C. Uher, *Appl. Phys. Lett.* 93, 252109 (2008).
23. K.F. Hsu, S. Loo, F. Guo, W. Chen, J.S. Dyck, C. Uher, T. Hogan, E.K. Polychroniadis, and M.G. Kanatzidis, *Science* 303, 818 (2004).
24. K. Biswas, J. He, Q. Zhang, G. Wang, C. Uher, V.P. Dravid, and M.G. Kanatzidis, *Nat. Chem.* 3, 160 (2011).
25. G.S. Nolas, J. Sharp, and H.J. Goldsmid, *Thermoelectrics: Basic Principles and New Materials Developments*, ed. A. Zunger, R. Hull, R.M. Osgood, and H. Sakaki (Berlin: Springer, 2001), pp. 1–288.